On the Single Porous Line Trailing Edge

P.C. Woodhead*, M.M. Scholz.† and T.P. Chong.‡
Brunel University London, Uxbridge, Middlesex, UB8 3PH, United Kingdom

P.F. Joseph§, P. Chatianya¶ and S. Palleja Cabre‖
Southampton University, Southampton, SO17 1BJ, United Kingdom

I. Nomenclature

ω	=	phase Angle
B	=	Baseline
$SINPLE$	=	Single Porous Line
L, x'	=	longitudinal displacement between two sources
U_∞	=	freestream velocity
c_0	=	chord length
f	=	frequency
z	=	span length
λ	=	wavelength
θ	=	porous hole diameter
p_{rms}	=	root mean squre pressure
P_0	=	reference pressure [= 20μ Pa]
SPL	=	sound pressure level
W	=	sound power integrated for the radiation angles
W_0	=	reference of sound power level [= 10^{-12}]
PWL	=	sound power level
c_∞	=	speed of sound [= 343 ms^{-1}]
ρ	=	air density [= 1.225 kgm^{-3}]
St	=	Strouhal number
Θ	=	polar angle
W	=	sound power integrated for the radiation angles

II. Introduction

Aerodynamic noise generated from the trailing edge of an aerofoil blade is a complex problem which poses a major environmental, health and operational issues. The research community has been continuously researching innovative solutions to further trailing edge self-noise reduction technologies. A particular inspiration come from owls known for their unique silent flight characteristics. Specifically, the unique characteristics found on the upper surfaces of the wings and feet being the soft and elastic downy [1] described as a form of porous structure.

The application of porous treatment for noise suppression dates to the 30s by Graham [1], who first studied the silent flight of the owl. Since then, significant progress has been made into the research of porous treatment for entire aerofoil, leading edge or trailing edge region to lessen aerodynamic noise. Geyer et al. [2] and Sarradj and Geyer [3] examined the noise characteristics of SD7003 aerofoil manufactured from various flow resistivity porous materials,

*Research Fellow, Department of Mechanical and Aerospace Engineering, philip.woodhead2@brunel.ac.uk, Non-member AIAA
†PhD Student, Department of Mechanical and Aerospace Engineering, max.scholz@brunel.ac.uk, Member of AIAA
‡Reader, Department of Mechanical and Aerospace Engineering, t.p.chong@brunel.ac.uk, Member of AIAA
§Professor, Institute of Sound and Vibration, pfj@isvr.soton.ac.uk, Member of AIAA
¶Lecturer, Institute of Sound and Vibration, c.c.paruchuri@soton.ac.uk, Member of AIAA
‖Research Fellow, Institute of Sound and Vibration, pfj@isvr.soton.ac.uk, Member of AIAA

including a non-permeable (solid) aerofoil as a reference. They observed noise reduction up to 10 dB, and greater was measured for the low to mid frequencies for porous aerofoils. However, they found that rougher surface texture of porous material contributed to the high frequencies noise increase. In addition, Sarradj and Geyer [3] examined the lift and drag performance of the porous aerofoil to the solid aerofoil. They found that the porous aerofoil generated a reduction in lift and an increased in drag compare to the non-porous aerofoil. However, they found that higher flow resistivity improved the lift and drag performance.

Since then, the research community has focused on limiting the porous treatment to the trailing edge. Geyer and Sarradj [4] demonstrated that limiting the porous treatment to the trailing edge resulted in further improvement in aerodynamic performance, while achieving appreciable noise reduction. They observed broadband noise reduction up to 8 dB, while a negligible reduction in lift and only 6% increase in drag for porous treatment applied to the last 5% of the chord length of the trailing edge. Rubio Carpio et al. [5] studied the porous inserts for the last 20% of the chord, at the trailing edge, for a NACA 0018 aerofoil. They found that a link between the flow permeability and noise reduction, where they observed noise reduction up to 7 dB and 11 dB for the higher permeability and lower permeability, respectively. It was also reported that they linked the permeability insert to:

1) the elongation in the streamwise direction result of the increase in the anisotropy of highly energetic, turbulent motions.
2) the reduction of eddy convection velocity.

Zhang and Chong [6] performed a sensitivity and parametric study of 3D printed structured-porous trailing edge inserts with several parameters, i.e., porosity, porous-size and porous coverage. They found that a mere 3.7% porous coverage of the chord resulted in a significant reduction of the turbulent broadband noise. It was also found that increasing the porous coverage offered slight improvement to the level of turbulent broadband noise reduction, but the reduction is less for small porous hole trailing edge. They concluded that the ideal case, small porous coverage, offered significant trailing edge self-noise reduction, in addition, potentially incurs minor aerodynamic penalties.

Herr et al. [7] and Delfs et al. [8] investigated the noise mechanism of porous trailing edge inserts and proposed that flow communication, as pressure fluctuation, between the pressure and suction surfaces of the porous trailing edge, refer to as pressure release process, was responsible for noise attenuation. Subsequent study by Rubio Carpio et al. [9] study the effect of permeable and non-permeable at the trailing edge. The non-permeable porous was filled with a thin layer of adhesive to form a solid membrane at the symmetry plane. They found that flow communication was necessary for noise attenuation at the trailing edge. It was also found that non-permeable porous insert was no longer reducing noise at low frequencies, however, high-frequency noise was unaffected due to the surface roughness. Furthermore, they confirmed the observation of pressure release process by the turbulent fluctuations in the boundary layer on both sides of the porous trailing edge remaining correlated.

Recent studies have investigated alternative methods of reducing aerodynamic noise through acoustic interference. A numerical study by Kim et al. [10] investigated the noise reduction mechanism employed on leading edge tubercle aerofoil. They observed reduction in the sound power level as a result of the surface pressure fluctuation at the leading edge, which was caused by the source cut-off effect along the oblique edge. They concluded that destructive interference between the peak and hill regions was one of the reasons for the noise reduction. A study by Chaitanya and Joseph [11] successfully demonstrated destructive interference mechanism between the root and tip of the slit. It was also found that an optimised slit leading edge could achieve leading-edge noise reduction up to 18 dB, compared to 7 dB for conventional sawtooth leading edge at 40 ms^{-1}.

The principle of phase cancellation has also been successfully shown for the trailing edge. A numerical study by Van der Velden et al. [12] investigated the link between the far-field noise and flow-field for a NACA-0018 aerofoil with a serrated trailing edge. They concluded that broadband noise reduction by the serrated trailing edge was attributed to the scattering of pressure waves along the oblique edges, resulting in acoustic interference. Experimental works by Woodhead [13] and Woodhead et al. [14] investigated acoustic interference through trailing edge modification to reduce turbulent trailing edge broadband noise. They successfully demonstrated acoustic interference between two sources that were physically displaced in the longitudinal direction. It also found that frequency tuning was achievable for the slit trailing edge. Furthermore, they developed an analytical noise prediction model based on acoustic interference, which was compatible with the experimental results. A further experimental work by Scholz et al. [15] examined acoustic interference with a single-row of porosity holes at the trailing edge of a NACA-0012 aerofoil. They established that acoustic interference could be achieved with a simplistic porous-arrangement at prescript distances from the trailing edge to reduce trailing edge noise without altering the boundary layer significantly.

Therefore, to summaries, the literature demonstrated that limiting the porous treatment to the trailing edge has advantage benefits in reducing aerofoil self-noise and well as lessens the aerodynamic penalty compared to full porous

aerofoil. Furthermore, the works by Scholz et al. [15] showed that adding a single row of porous holes could reduce noise through acoustic interference, while not altering the boundary layer. The main objective of this paper, therefore, is to perform an experimental study to further extend the works by Scholz et al. [15] into the characteristic and mechanisms of Single Porous Line, SINPLE, with different configuration. This paper will study the effects of SINPLE trailing edge on the far-field radiation, unsteady pressure and boundary layer near the trailing edge at various freestream velocities and at a low angle of attack.

Wave Theory

The fundamental of this work is based on the interference from wave theory. The principle for this paper is that the trailing edge geometry facilitates acoustic interference between two sources that are physically displaced in the longitudinal direction. Essentially, an incoming turbulent eddy scatters into noise at the first scattering location, where it continues to propagate downstream to the second scattering location. This result in acoustic scattering to occur at different locations in time from the same hydrodynamic distribution. The difference in the acoustic waves result in a phase angle, $\hat{\omega}$, which can be described by a generic term, defined as:

$$\hat{\omega} = \frac{\omega L}{U_\infty} \tag{1}$$

$$\omega = 2\pi f \tag{2}$$

where f is frequency, L is longitudinal displacement between the two sources and U_∞ is the freestream velocity. Note that L is defined as x' as shown in Figure 4b.

To attain perfect destructive interference, two coherence sources, S1 and S2, emitted acoustic waves at 180° out-of-phase. The phase difference, phase angle, can be expressed as $n\pi$, where n = 1 , 3 , 5 and so on. This results in cancellation of the acoustic sound waves. In contrast, a perfect constructive interference occurs when two coherence sources emitted acoustic waves in phase (i.e. when n = 2, 4, 6 and so on), which results in the amplification of the acoustic waves to the far-field. In the case of the trailing edge the time taken for the turbulent eddies to convection between the two scattering locations which results in the phase difference.In particular for this case, the convection of the turbulent eddies should instead be used rather than freestream velocity based on the observation from Woodhead [13] and Scholz et al. [15]. Therefore, to summaries:

$$\frac{2\pi f x'}{U_c} = n\pi \tag{3}$$

$$St = \frac{f x'}{U_\infty} = \frac{1}{2} n \begin{cases} n = 1, 3, 5, \ldots & \text{for destructive interference} \\ n = 2, 4, 6, \ldots & \text{for constructive interference} \end{cases} \tag{4}$$

where St is known as the Strouhal number, which demonstrates that the respective values of the non-dimensional frequency at which the destructive acoustic interference occurs at 0.5, 1.5, 2.5 and so on, and the constructive interference occurs at 1, 2, 3 and so on. It is therefore possible to tune a particular incoming velocity where the value of x' dictates the frequency characteristics by the destructive interference (as well as the constructive interference).

III. Experimental set-up

A. Design of the experimental aerofoil and interchangeable trailing edges

The experimental aerofoil used within this research is the NACA-0012 symmetrical aerofoil. The overall span length of the aerofoil is 0.38 m, where only 0.3 m is within the working section of the open jet wind tunnel, and the remaining being the mounting plates to the open jet nozzle side plates. The experimental aerofoil is composed of two parts: main aerofoil body and the interchangeable trailing edges. The overall chord length of the aerofoil is c_0 = 0.15 m, where the main aerofoil body chord-length is 0.1 m and the interchangeable trailing edge is 0.05 m. The interchangeable trailing edge and the main aerofoil body interlock via a hook slot joint, which allows for a tight fit. In addition, a unsteady pressure trailing edge configuration, illustrated in Fig. 4b., has four evenly position taps at 1.5 mm intervals in the streamwise direction on either side of the porous hole with embedded tube exit to one side. The aerofoil and trailing edges are 3D printed with a resolution of 35 microns (0.035 mm).

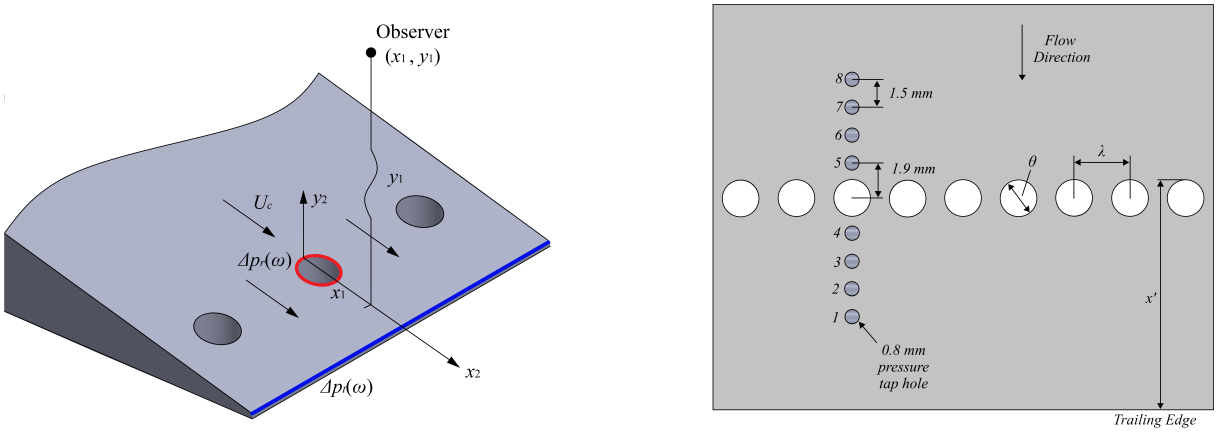

(a) **(b)**

Fig. 1 Topology of the Single Porous Line, SINPLE, trailing edge where (a) assumption applied to the analytical model where the sources are define as: red - porous hole source and blue - tip source, and (b) geometric parameters and unsteady pressure tap locations

Figure 4b showcases the geometric parameters for the trailing edge. The four geometric parameters are the longitudinal displacement (x'), wavelength (λ), hole diameter (θ), and hole angle (ϕ). The baseline (non-porous) trailing edge and single porous line trailing edge will denoted as B and SINPLE, respectively. These acronyms are used throughout the paper. The coordinate system is defined as follows: streamwise (x), vertical (y) and spanwise (z).

Coarse sandpaper strips are applied to both the suction and pressure surfaces of the aerofoil at $x/c_0 = 0.2$ to trip the boundary layer into turbulent. This is to ensure that turbulent noise source can be generated at the trailing edge. The coarse sandpaper has a thickness of 0.95 mm and width of 10 mm.

This paper investigates several geometrical parameters, illustrated in Figure 4b, longitudinal displacement (x'), wavelength (λ), hole diameter (θ), and hole angle (ϕ). The range of each parameter is as follows: 3 mm $\leq x' \leq$ 28.8 mm, 3 mm $\leq \lambda \leq$ 15 mm, 0.7 mm $\leq \theta \leq$ 3 mm, and 0.7° $\leq \phi \leq$ 3°.

B. Wind tunnel facilities and instrumentation

This section describes the wind tunnel facilities and instrumentation set-up for the far-field noise, hot-wire anemometry and unsteady pressure measurements, which are performed at the aero-acoustic facility at Brunel University London. The facility consists of an open jet wind tunnel located within 4 m × 5 m × 3.4 m anechoic chamber. The exit of the open jet nozzle is 0.10 m in width by 0.30 m in height. The open jet wind tunnel is capable reaching U_∞ = 80 ms^{-1}, however, this current works will only operated between U_∞ = 20 ms^{-1} to U_∞ = 60 ms^{-1} at intervals of 2 ms^{-1}, where these corresponds to Reynolds number of 2.03×10^{-5} to 6.09×10^{-5}, respectively. The open jet wind tunnel can produce low turbulence intensity of 0.1 % - 0.2 % at $U_\infty \approx$ 30 ms^{-1}. The background noise (without he presence of the aerofoil, but with the side plates in place) is largely contributed by the low subsonic jet noise, which is very low in comparison to the aerofoil self-noise level produced at the identical flow speed. All the far-field noise, hot-wire anemometry, and unsteady pressure measurements are performed at a geometric angle of attack of $\theta = 0°$.

The far-field noise measurements were obtained using eight G.R.A.S $^1/_2$" condenser microphones (46AE). The microphones are positioned at 50° $\leq \Theta \leq$ 120° at intervals of 10°, at radius of r = 0.97 m above the mid-span of the aerofoil trailing edge. The noise signal is acquired through a 24-bit PXIe-4464 analogue-digital card manufactured by National Instruments, where a gain of ± 20 dB is automatically applied. The sampling frequency is 44 kHz and a sampling time of 20 seconds. The sampled data is windowed and the Power Spectral Density (PSD) of 1 Hz bandwidth is computed from a 1024-point Fast Fourier Transformation (FFT) with a frequency resolution of 39 Hz and a 50% overlap time.

The Sound Pressure Level, SPL, is expressed by the following equation:

$$\mathrm{SPL}(f) = 20\log_{10}\left[\frac{p_{rms}}{P_0}\right], \mathrm{dB} \tag{5}$$

where p_{rms} is the root mean square of the acoustic pressure and P_0 is the reference pressure being 20μ Pa. The Sound Power Level, PWL, is calculated based on the assumption that the acoustic waves radiated in spherical fashion from the trailing edge. The PWL radiated per unit span in the range of polar angles between is calculated by the following equations:

$$W(f) = \frac{2\pi \int S_{pp}(f,\Theta)\Delta\Theta}{\rho c_\infty} \tag{6}$$

$$\mathrm{PWL}(f) = 10\log_{10}\left[\frac{W(f)}{W_0}\right], \mathrm{dB} \tag{7}$$

where S_{pp} is the far-field pressure power spectrum density at a polar angle Θ, where $\Delta\Theta = 10^\circ \times \frac{\pi}{180}$ is the angle between adjacent microphones in radian, and $W(f)$ is the sound power integrated for the radiation angles from Θ_1 to Θ_8, with intervals of 10°, $W_0 = 10^{-12}$ W, $c_\infty = 343$ ms^{-1} is the speed of sound for air and $\rho = 1.225$ kg/m^3 is the air density. The overall sound power level (OAPWL) of the aerofoil self-noise defined within a frequency range f can be represented by:

$$\mathrm{OAPWL} = 10\log_{10}\left[\frac{\int_f W(f)df}{W_0}\right], \mathrm{dB}. \tag{8}$$

The study of the flow velocity measurement within the boundary layer of the baseline and SINPLE trailing edges were acquired with both single wire hot-wire probe and cross-wire (X-wire) hot-wire probe. The single wire hot-wire (55P11) is used to acquire the mean and fluctuating velocities, whereas, the X-wire (55P61) is used to measure two-component velocity fluctuations u' and v'. Both hot-wires were operated at a over-heat ratio of approximately 1.8, which ensure a good velocity sensitivity in the flow measurements. The hot-wire signals are digitised by a 16-bit A/D convector unit at a sampling frequency of 20 kHz. A DANTEC Dynamic Multichannel Constant Temperature Anemometer (CTA) 54N80 was used and allowed adjustment to the voltage offset and gain of the hot-wire signal to the A/D. The hot-wire readings were recorded through DANTEC StreamWare software. The hot-wire probe were mounted on a three-dimensional traverse plotter with a resolution of 0.01 mm in all three directions.

The unsteady pressure measurements were acquired with eight pressure tap holes along the trailing edge. The pressure taps are connected, via silicon tubing, to a Knowles FG3229-P07 electret condenser microphones with a diameter of 2.57 mm and sensor diameter of 0.8 mm. An additional 3 m of silicon tubing is connected to the other end of the acrylic holder where it ends outside the working section of the open jet wind tunnel. The extensive length of silicon tubing is to ensure that no backward reflection from the sudden termination of acoustic wave, whilst ensuring that the acoustic waves reach the remote microphones. The unsteady pressure signal is acquired using a 16-bit analogue-digital card manufactured by National Instruments. The signal is recorded at a sampling frequency of 40 kHz with a sampling time of 30 seconds. The data were windowed and the PSD of 1 Hz bandwidth was computed from a 1024 point FFT and a 50 % overlap time. A transfer function estimation represents the ratio between the input and output signals in the frequency domain. Therefore, the input signal can be obtained by multiplying the transfer function to the output signal. The definition of the transfer function estimation, $H(f)$, is given as:

$$H_{RMP}(f) = \frac{E[V_{RMP}(f)V^*_{ref}(f)]}{E[V_{ref}(f)V^*_{ref}(f)]} \tag{9}$$

where $E[V_{RMP}V^*_{ref}]$ is the cross spectra density between the signal inputs of the remote microphone position, RMP, and the reference microphone and $E[V_{ref}V^*_{ref}]$ is the auto spectra density of the reference microphone. Within this approach also obtains the phase information of each remote microphone used in the measurement of the surface pressure fluctuations over the frequency range. The frequency response of the remote microphone is acquiring the signal from the 1/4" G.R.A.S condenser microphone as the input signal, as well as from the remote microphone as the output signal. The calibration is performed using white noise signal used with a loudspeaker through a cone pressed against the surface above the pressure taps.

IV. Results

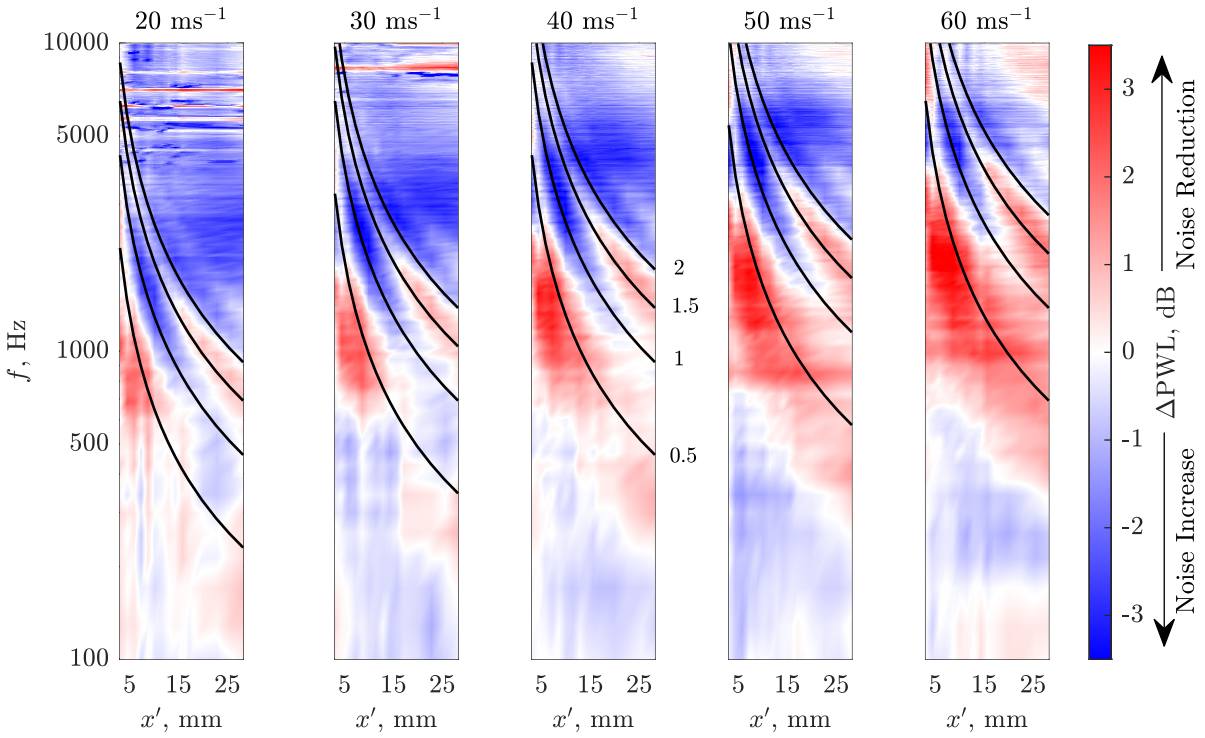

Fig. 2 Contour map of the ΔPWL, dB, between the SINPLE and baseline trailing edge at 3 mm $\leq x' \leq$ 28.2 mm, at 20 ms^{-1} $\leq U_\infty \leq$ 60 ms^{-1} with intervals of 10 ms^{-1} and the wavelength (λ) is kept at 3 mm.

The result, as shown by Figure 2, shows the contour of ΔPWL at various longitudinal displacement, x', against frequency, f, at 20 ms^{-1} $\leq U_\infty \leq$ 60 ms^{-1} at intervals of 10 ms^{-1}. ΔPWL is defined as a difference in the sound power levels, as a function of frequency, between B and SINPLE trailing edges. Note that positive ΔPWL represents noise reduction, and the opposite is true for negative ΔPWL being noise increase. The results clearly demonstrate and validify the co-existence of destructive and constructive interference regions across all freestream velocities and longitudinal displacements. In addition, the peak noise reduction correlated well with the curve pertaining to the non-dimensional frequency of St = 0.5 and St = 1.5, which corresponds to destructive interference between the single row of porous holes and the trailing edge. Similarly, observation of noise increases due to constructive interference at St = 1 and St = 2. The convection velocity was $0.65U_\infty$, this was obtained and discussed further within this paper.

In terms of sound power level, PWL, the level of noise reduction can be seen to improve with freestream velocity from 2 dB to 4 dB at U_∞ = 20 ms^{-1} and U_∞ = 60 ms^{-1}, respectively. At U_∞ = 20 ms^1, the noise reduction was only limited to the smaller longitudinal displacements $x' \leq$ 11.4mm, in comparison to U_∞ = 60 ms^{-1} observed noise reduction across all x' within this study. However, for all freestream cases, the highest noise reduction was consistently observed at the small longitudinal displacement, as well as the highest noise increase.

As explained in Sec.II, this mechanism requires the same turbulent eddies, ideally perfectly coherent, to scatter into pressure waves at different locations in time. However, the turbulent eddies develop over time along the surface of the aerofoil, as a result the coherent strength between the first and second scattering locations degrades. This can be seen with the degradation of the noise reduction at St = 0.5 and 1.5 towards larger x' as the freestream velocity is reduced.

It was also observed in Figure 2 region of broadband noise increase at the mid-to-high frequency for the larger longitudinal displacement. Furthermore, the region of broadband noise increase is associated to the at higher freestream velocity, it was observed that the increase noise level is seen to However, at the higher freestream velocity exhibit a reduction in the noise increase.

A. Analytical Model for SINPLE

Based on the wave theory from Section II, a simple analytical model that can predicted the destructive (noise reduction) and constructive (noise increase) interference for the SINPLE trailing edge. A schematic, shown in Figure 4a, of the SINPLE trailing edge geometry shows the two compact sources, at the porous hole and the trailing edge, where the implementation of the strong acoustic interference will take place between the sources. The incoming turbulent eddies interacts with the porous hole resulting in a localise source at $y_1 = 0$, where it generates a pressure difference fluctuation denoted as $\Delta p_h(\omega)$. The same turbulent eddies propagate downstream over the surface of the aerofoil at convection velocity, U_c. After a period of time, the turbulent eddies will interact with the trailing edge resulting in a secondary localised source, at $x_2 = x'$, where it generates a secondary pressure difference fluctuation denoted as $\Delta p_t(\omega)$. Therefore, the analytical model assumes that the two compact sources strength defined as $\Delta p_r(\omega)$ (porous hole - red line) and $\Delta p_t(\omega)$ (trailing edge - blue line) is used to calculate the source distribution along the SINPLE trailing edge. A Dirac delta function is used to represented the two source locations: single row holes and the trailing edge. This function can be assumed as the source distribution into the radiation integral of Amiet trailing edge noise model [16] gives the following:

$$p(x_1, y_1, \omega) \sim \frac{x_1}{4\pi c_\infty \sigma} \int_0^H (\Delta p_r(\omega)\delta(0) + \Delta p_t(\omega)\delta(H))\, e^{\left(-i\left(\frac{\omega}{c_\infty \beta^2}\right)\left(\frac{M-x_1}{\sigma}\right)x_2\right)} - dx_2 \tag{10}$$

$$\sigma^2 = x_1^2 + \beta^2 y_1^2 \tag{11}$$

$$\beta^2 = 1 - M^2 \tag{12}$$

A assumption is made that the adjacent porous holes are further apart than the turbulence length scale, so interaction between the same eddies to multiple porous holes does not occur. The power spectrum density of the unsteady wall pressure for each hole can be summed up without regard to the phase difference. After performing the integration over the longitudinal displacement x', the following expression can be obtained:

$$p(x_1, y_1, \omega) \sim \frac{x_1}{4\pi c_\infty \sigma} \left(\Delta p_r(\omega) + \Delta p_t(\omega)) e^{\left(-i\left(\frac{\omega}{c_\infty \beta^2}\right)\left(M - \frac{x_1}{\sigma}\right)\right)H} \right) \tag{13}$$

Consider the power spectra density of far-field pressure radiation,

$$\begin{aligned} S_{pp}(x_1, y1, \omega) &= E[p(x_1, y_1, \omega)p^*(x_1, y_1, \omega)], \\ S_{pp}(x_1, y1, \omega) &= \left(\frac{x_1}{4\pi c_\infty \sigma}\right)^2 \left[S_{\Delta p_{rr}}(\omega) + S_{\Delta p_{tt}}(\omega) + E[\Delta p_r(\omega)\Delta p_r^*(\omega)] e^{\left(\frac{i\omega(M-\frac{x_1}{\sigma})H}{c_\infty \beta^2}\right)} \right] \end{aligned} \tag{14}$$

The term $E[\Delta p_r^*(\omega)\Delta p_t(\omega)]$ (and its conjugate) is the boundary layer streamwise cross spectrum, which may be expressed in complex form:

$$E[\Delta p_r^*(\omega)\Delta p_t(\omega)] = \sqrt{(S_{\Delta p_{rr}}(\omega)S_{\Delta p_{tt}}(\omega))}\gamma\left(\frac{\omega H}{l_1(\omega)}\right) e^{\left(-\frac{i\omega H}{U_c(\omega)}\right)} \tag{15}$$

where $\gamma(\frac{\omega H}{l_1(\omega)})$ is the boundary layer streamwise (purely real) coherence function, assumed to be a function of the ratio of streamwise longitudinal distance x' to frequency-dependent coherence length $l_1(\omega)$. Note that the phase $\frac{\omega H}{U_c(\omega)}$ of the cross spectrum is assumed to originate solely from the time taken for the turbulent eddies to convect over the longitudinal displacement x', where $U_c(\omega$ is the frequency-dependent convection velocity. Following Corcos:

$$\gamma\left(\frac{\omega H}{l_1(\omega)}\right) = e^{\left(-\frac{\eta \omega H}{2U_c(\omega)}\right)} \tag{16}$$

provides an acceptable fit to the measured streamwise coherence function shown in Corcos [17, 18], where η is the empirical constant $\eta = 0.14$. The following Corcos empirical fit to the frequency-dependent convection velocity between two points separated by x_2 is given by,

$$\frac{U_c(\omega)}{U_\infty} = -9.6 \times 10^{-6} f + 0.5 \left(1 + \frac{x_2}{\delta^*}\right)^{0.16} \tag{17}$$

Combining the Eqn. 16, the far-field radiated pressure PSD may be expressed in the form:

$$S_{pp}(x_1, y_1, \omega) = (\frac{x_1}{4\pi c_\infty \sigma})^2 (S_{\Delta p_{rr}}(\omega) + S_{\Delta p_{tt}}(\omega)) + 2\sqrt{S_{\Delta p_{rr}}(\omega) + S_{\Delta p_{tt}}} e^{\left(-\frac{\eta\omega H}{2U_c(\omega)}\right)} \cos\left(\omega(\tau_H + \tau_A)\right) \tag{18}$$

where τ_H is the time taken for the turbulent eddies to convect along the longitudinal displacement,

$$\tau_H = \frac{H}{U_c(\omega)} \tag{19}$$

and τ_A is the difference in propagation times to the observer between sound radiation at the hole of the SINPLE trailing edge and the trailing edge of the aerofoil,

$$\tau_A = \frac{H}{c_\infty \beta^2} \left(\frac{M - x_1}{\sigma}\right) \tag{20}$$

which may be expressed in terms of observer angle θ by putting $x_1 = r\cos\theta$ and $x_2 = r\sin\theta$

$$\tau_A(\theta) = \frac{H}{(c_\infty \beta^2)} \left(\frac{M - \cos\theta}{\sqrt{(\cos^2\theta + \beta^2 \sin^2\theta}}\right) \tag{21}$$

Note that at the peak frequency ω_0 where $\frac{(\omega_0 H}{U_c} = \pi$.

$$\begin{aligned} S_{pp}(x_1, y_1, \omega_0) = &\left(\frac{x_1}{4\pi c_\infty \sigma}\right)^2 \left(S_{\Delta p_{rr}}(\omega_0) + S_{\Delta p_{tt}}(\omega_0)\right) \\ &+ 2\sqrt{S_{\Delta p_{rr}}(\omega_0) S_{\Delta p_{tt}}(\omega_0)} e^{\left(-\frac{\eta\omega H}{2U_c(\omega_0)}\right)} \cos\left(\omega_0(\tau_H + \tau_A)\right). \end{aligned} \tag{22}$$

The evaluation of the analytic model to experimental results are shown in the next section. Readers should be aware that the analytic model should be used to predict the noise trends at which the peak frequency occurs, and not to predict the noise reduction. The prediction of the noise reduction requires additional information to estimate the source strength located at the porous hole and trailing edge, $S_{\Delta prr}$ and $S_{\Delta ptt}$. The analytic result assume that the source strength between the root and tip are at the most effective interference. As a result, for the purpose of the comparison to the experimental results at various freestream velocity and longitudinal displacement, this assumption will be used.

The next investigation evaluated the coherence length obtained by a comparison of the Corcos empirical model to experimental coherence. The term 'coherence length' describes the rate of the decay calculated using the square root coherence function [19]. The coherence length for two separate readings in the streamwise or spanwise direction, η_x and η_z respectively, was obtained by fitting an exponential to the square root coherence γ at $\eta_{x,z}$. Corcos [17, 18], proposed, subsequent modified by Finnveden *et al.* [20], the empirical model approach given as:

$$\gamma(\omega, \eta_x, \eta_z) = e^{\left(-b_1 \frac{\omega\eta_z}{U_c}\right)} \cdot e^{\left(-b_3 \frac{\omega\eta_x}{U_c}\right)} \cdot e^{i\left(\frac{\omega\eta_z}{U_c}\right)}, \tag{23}$$

$$\gamma(\omega, \eta_x) = e^{\left(-b_3 \frac{\omega\eta_x}{U_c}\right)}, \tag{24}$$

$$\gamma(\omega, \eta_z) = e^{\left(-b_1 \frac{\omega\eta_z}{U_c}\right)}, \tag{25}$$

where b_1 and b_3 are the decay factors for spanwise and streamwise respectively. The spanwise and streamwise coherence lengths are defined in Eqn.23 as the first two exponential terms, and the third exponential term accounts for the mean pressure field [21]. The streamwise and spanwise coherence lengths are defined a Eqn.24 and Eqn.25, respectively.

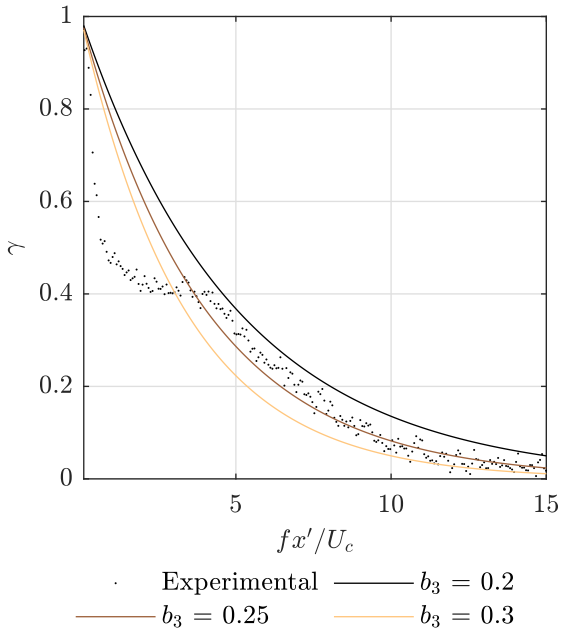

Fig. 3 Comparison of the Corcos Empirical model for streamwise coherence to the experimental streamwise coherence γ at U_∞ = 40 ms^{-1}

Figure 3 presents a comparison of the Corcos Empirical model, defined in Eqn. 24, and the experimental for streamwise coherence against non-dimensional frequency, $\frac{fx'}{U_c}$, at U_∞ = 40 ms^{-1}. The experimental magnitude squared coherence is defined in Eqn. 26 for pressure taps at positions 2 and 5 shown in Figure 4a. It can be obtained from Figure 3 that a good agreement between the experimental coherence and the Corcos Empirical model for decay factor b_3 = 0.25 for $\frac{fx'}{U_c} \geq 4$.

$$\gamma^2(f) = \frac{|E[V_x(f)V_y^*(f)]|^2}{E[V_x(f)V_x^*(f)] \cdot E[V_y(f)V_y^*(f)]} \tag{26}$$

In previous studies [13–15] the convection of the turbulent eddies should be used rather than the freestream velocity. Therefore, the analysis is performed at the time domain by calculating the cross-correlation coefficients between the pressure taps between 5 to 2 (refer to Fig. 4a). The results are displayed in Figure 4 for both the baseline and SINPLE trailing edges. An arbitrary threshold is used to discretion the dominant cross-correlation coefficients from the non-dominant ones. The convection velocity, U_c, is calculate by the gradient in the form of $\eta_x/\Delta\tau$. The non-dimensional convection velocity is defined as a fraction of the local freestream velocity where the baseline and SINPLE trailing edge were 0.7 and 0.6485, respectively.

B. Comparison between experimental and predicted noise by SINPLE trailing edge

The following analysis evaluates the noise prediction model, based on Eqn. 23, to the experimental results at various freestream velocities (U_∞) shown in Figures 5aand 5b, respectively. The experimental SPL corresponds to polar angle of 90° positioned above the trailing edge. The acoustic interference is described by the non-dimensional frequency, in accordance to Eqn. 4. Note that the following parameters and condition were applied to the prediction model: convection velocity and decay factor are U_c = 0.6485 and μ = 0.25, respectively, and source strength is assumed to be perfect between the porous hole and trailing edge, unless stated otherwise.

Figure 5 presents the difference in Sound Pressure Level (ΔSPL) to the non-dimensional frequency for longitudinal displacements, 3 mm $\leq x' \leq$ 28.2 mm, where wavelength, hole diameter and freestream velocity were kept at λ = 3 mm, and θ = 2 mm, and U_∞ = 50 ms^{-1}, respectively. The results showed that the model is capable of capturing the peaks (destructive interference) and troughs (constructive interference) at St = 0.5 and 1.5 and St = 1 and 2, respectively, across a wide range of longitudinal displacements. However, the noise level of the experimental result was not able to be capture by the model with over estimated at the mid-to-high frequencies. The results, shown in Fig. 5a, also exhibited noise reduction at 950 Hz < f < 1500, corresponding to St = 1, for x' > 16 mm and noise increase at f > 1500

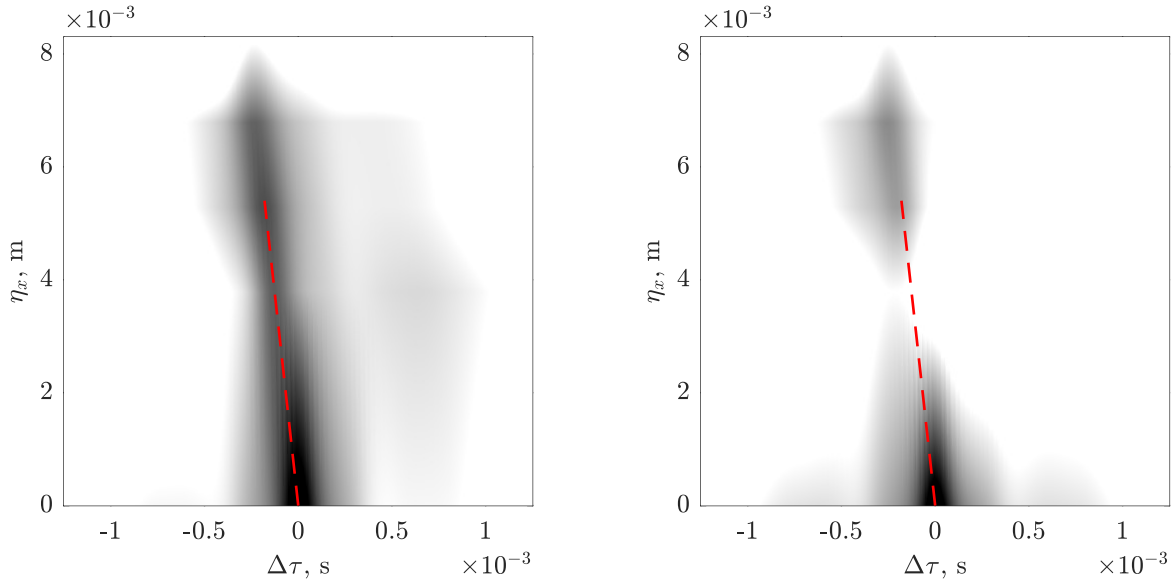

(a) Baseline **(b) SINPLE**

Fig. 4 Comparison of the convection velocity of the SINPLE to the Baseline trailing edge at x' = 11.4 mm, λ = 3 mm and θ = 2 mm, at U_∞ = 40 ms^{-1} and between pressure taps 5 to 1.

Hz, corresponding to *St* = 1.5, for 20 mm > x'. As it is assumed that firstly the source strength is perfectly coherent between the two sources resulting in the maximum noise levels produced by acoustic interference, and secondly that the analytical model is only modelling the phase cancellation mechanism. Therefore, this model should only be assumed to provided a prediction of the trends.

Up to this point, the source strength is assumed to be perfectly coherent between porous hole and the trailing edge. The result, as shown in Figure 3, clearly demonstrates a loss of coherence between the pressure taps 5 and 1 against non-dimensional frequency. Therefore, the coherence result obtained in Fig. 3 is used to describe the source strengths between the two scattering locations: porous hole and trailing edge illustrated in Fig. 4a. Figure 6 presents a comparison between the analytical model to experimental results for x' = 11.4 mm, λ = 3 mm, and θ = 2 mm, at U_∞ = 30 ms^{-1} and 60 ms^{-1}. The result showed good agreement between the experimental to analytical model with the model correctly predicting peaks (destructive) and toughs (constructive) trends generated by the acoustic interference up to *St* = 2.5. Furthermore, the over-prediction of the acoustic interference observed in Figure 5 at mid-to-high frequency is no-longer observed in Figures 6, which provide a good representation of the noise levels solely the result of the acoustic interference. However, this model is unable to provide a realistic prediction as other noise component such as aerofoil self-noise contributed to the overall noise characteristics seen for the SINPLE trailing edge.

C. Noise Performance of SINPLE trailing edge

1. Variation in the SINPLE longitudinal displacement

The application of adding a single line of porous holes at a prescribe longitudinal displacement, as shown in Figure 2, successfully resulted in phase cancellation with the co-existence of destructive and constructive interference been observed. Next, the effects of longitudinal displacement, x', on the difference in sound power level, ΔPWL, in comparison to baseline, is showcased in Figures 7a and 7b, at U_∞ = 40 ms^{-1} with the following observations:

1) At *St* = 0.5, the results clearly showed that a significant reduction in noise levels can be achieved by SINPLE trailing edge, with the largest reduction was observed at x' = 4.4 mm with reduction up to 3.5 dB. However, the level of noise reduction achieved tended to degrade with increase of longitudinal displacement, with the lowest reduction achieved by x' = 22.6 mm with only 0.5 dB reduction. Followed by a slight improvement in noise reduction was observed for the largest x' = 28.2 mm with reduction of 1 dB.
2) At *St* = 1, the noise levels degraded further until x' = 8.6 mm with noise increase of 3.8 dB. It was then followed

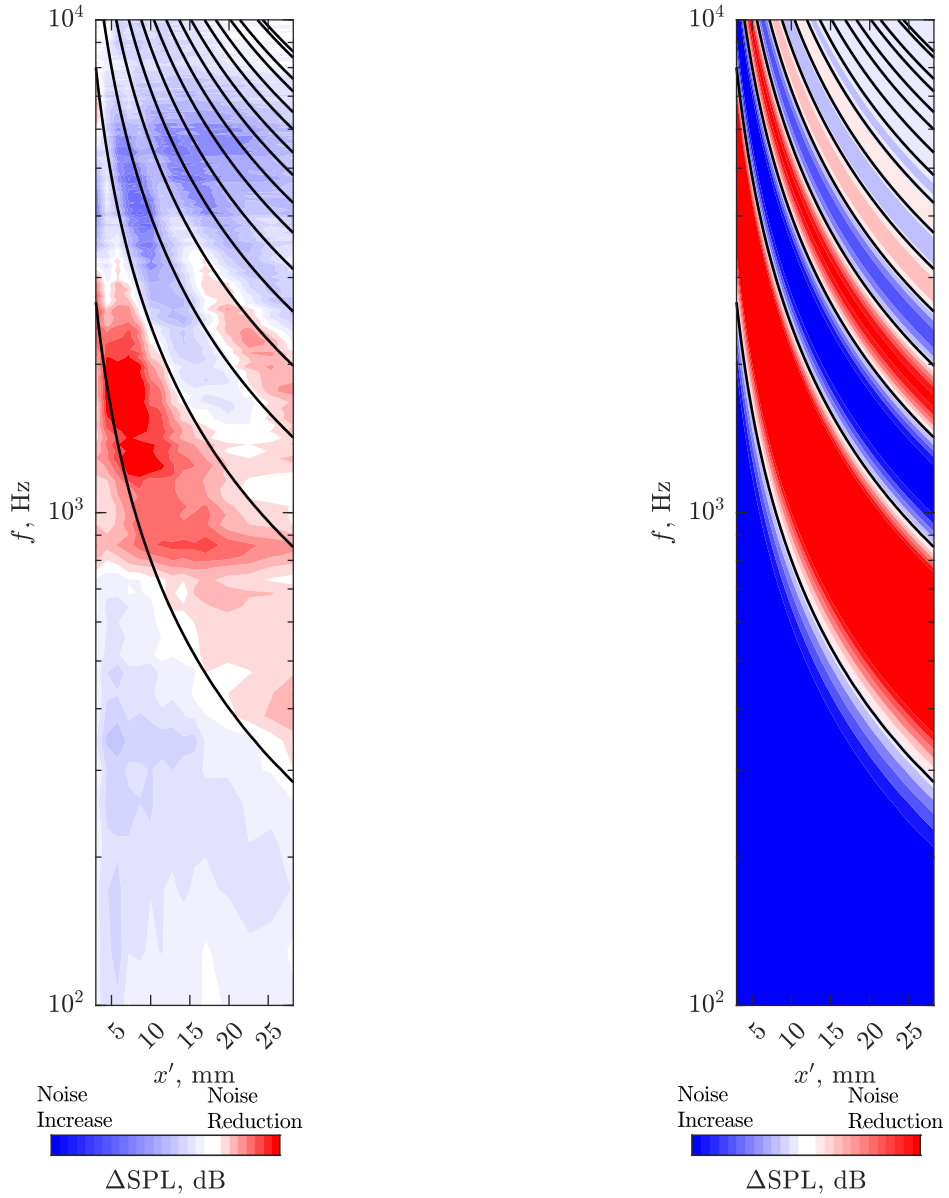

Fig. 5 Comparison of the ΔSPL, dB, of the analytical model to experimental results for (a) the longitudinal displacement at x' = 10 mm, 19.8 mm and 28.2 mm and (b) the freestream velocity for x' = 10 mm at U_∞ = 20 ms^{-1}, 40 ms^{-1} and 60 ms^{-1}, where λ = 3 mm and θ = 2 mm.

by enhancement in the noise level with largest x' only producing 0.5 dB of noise increase, in comparison to the baseline.

3) At St = 1.5, similar observation to St = 1 with the noise levels degrading from 0.5 dB to 2 dB noise increase for x' = 3 mm and 10 mm, respectively. At $x' \geq$ 10 mm, the level of noise significantly improves with SINPLE trailing edge cases achieving noise reduction up to 1.5 dB.
4) At the smaller longitudinal displacement, $x' \leq$ 8.6 mm, presented a interesting observation where the PWL spectrum no longer collapse at St = 0.5, 1, 1.5, and 2. The following reason could explain this:
    - Interaction of the turbulent structure with the porous hole and trailing edge with the combined effect of a reduced convection velocity along the trailing edge due to the pressure gradient, result in the time taken to be longer than other cases upstream with higher average convection velocity.

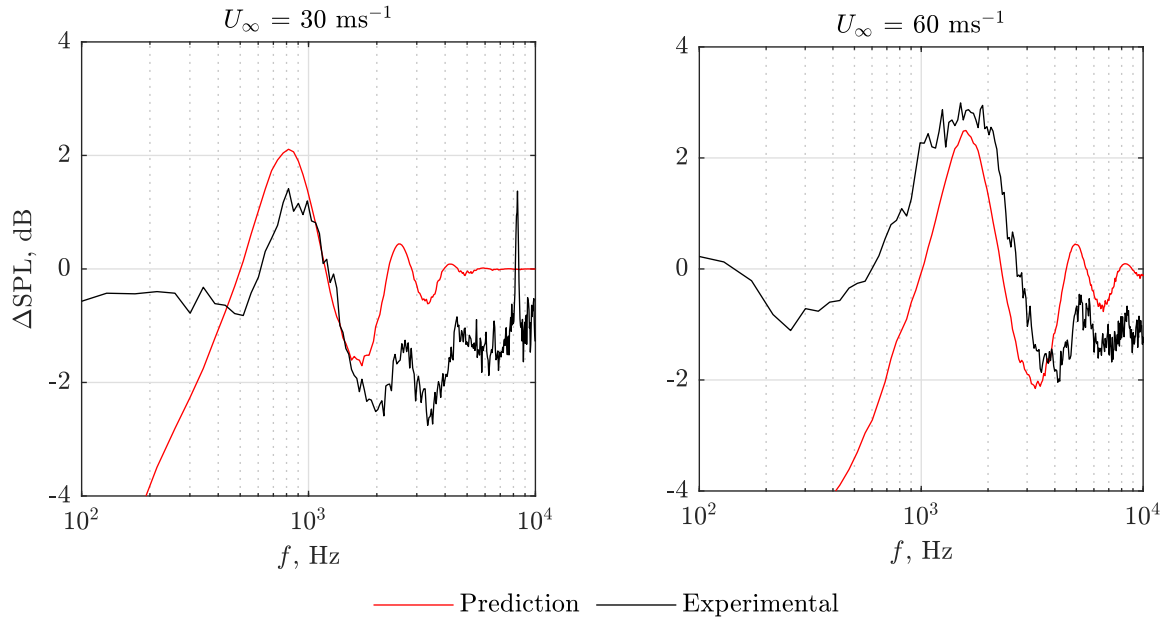

Fig. 6 Comparison of the ΔSPL, dB, of the analytical model based on the source strength to experimental results for x' = 11.4 mm, λ = 3 mm and θ = 2 mm at U_∞ = 40 ms^{-1}

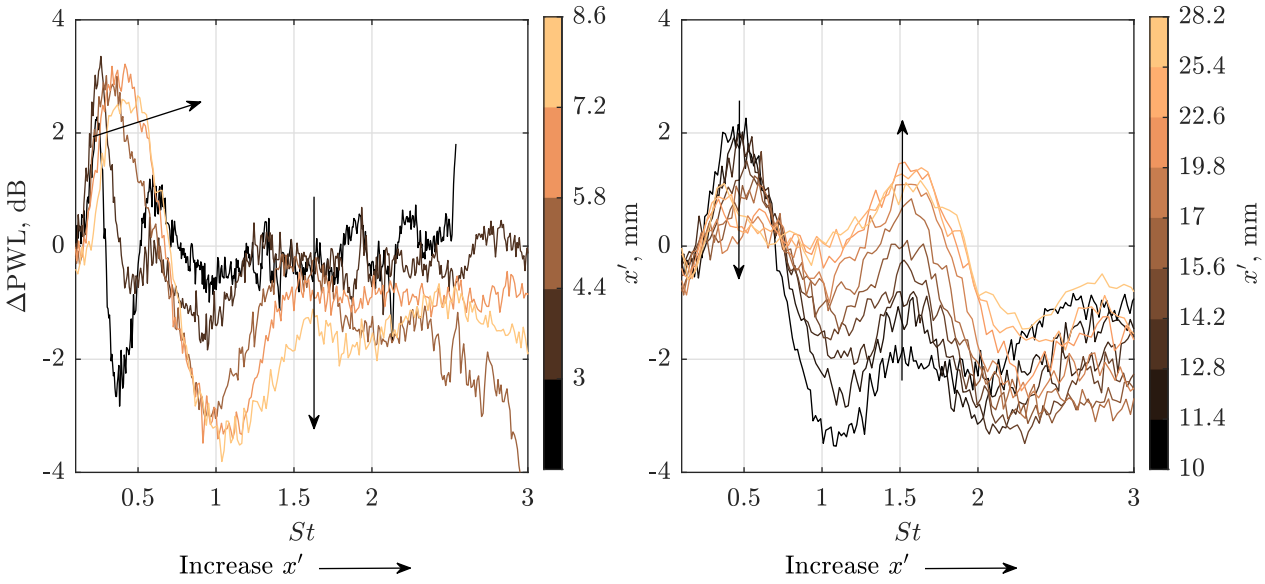

(a) 3 mm ≤ x' ≤ 8.6 mm **(b) 10 mm ≤ x' ≤ 28.2 mm**

Fig. 7 Comparison of the ΔPWL, dB, between the baseline and SINPLE trailing edge where a. 3 mm ≤ x' ≤ 8.6 mm, and b. 10 mm ≤ x' ≤ 28.2 mm, at λ = 3mm, and θ = 2 mm, at U_∞ = 40 ms^{-1}

2. Variation in the SINPLE wavelength

The effects of wavelength, λ, on the ΔPWL at different longitudinal displacement, x' is investigated. The result, in Figure 8, demonstrated that increasing the wavelength has a significant influence on the effectiveness on the acoustic interference by the SINPLE trailing edge. Firstly, the results showed that increasing the wavelength between scattering locations reduced the effectiveness of phase cancellation between the two scattering locations being the trailing edge and the single row of holes. This observation is clearly showcase in Figure 8 for x' = 4.4 mm with the highest level of noise reduction up to 3.8 dB produced by the smallest λ = 3 mm, compared to the largest λ = 15 mm only achieving 1.8

dB. Similarly, the constructive interference was enhanced with wavelength with the smallest λ = 3 mm achieving the largest noise increase of 2 dB in comparison to λ = 15 mm which achieved 1 dB and these observation were seen for all x' cases and all freestream velocities. Therefore, the number of scattering locations along the trailing edge has a significantly effect the likelihood of acoustic interference to occur and the noise level. Furthermore, the results clearly showed that the wavelength has no effect on phase cancellation between the porous holes in the spanwise direction with the collapse of the noise spectrum.

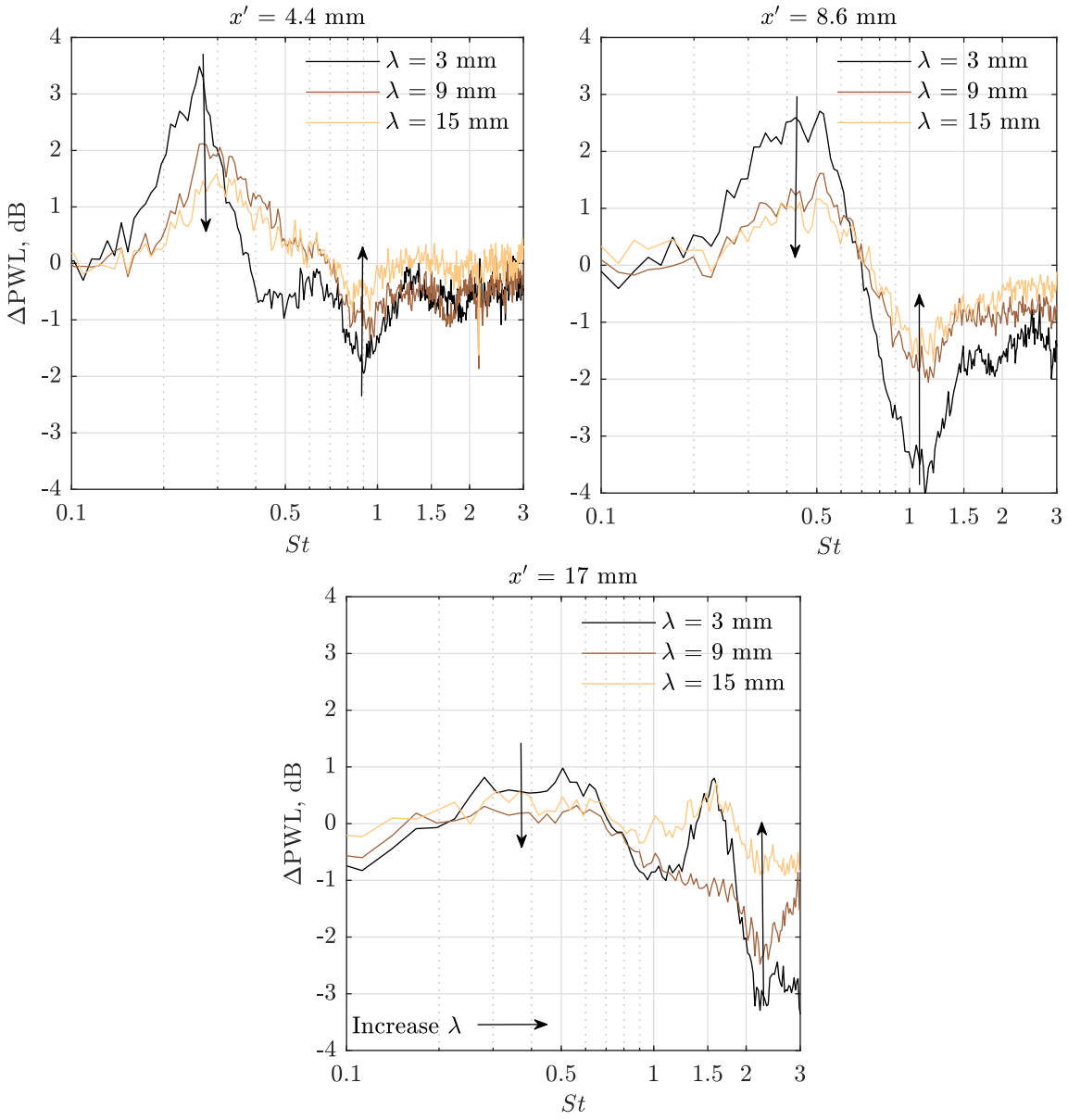

Fig. 8 Comparison of the ΔPWL, dB, between B and SINPLE trailing edge at x' = 4.4 mm, 8.6 mm and 17 mm, and λ = 3 mm, 9 mm and 15 mm; where θ = 2 mm and U_∞ = 40 ms^{-1}.

3. Variation in the SINPLE Hole Diameter

Next, Figure 9 presents the difference in sound power level to the frequency for porous hole diameter, θ, of 0.7 mm $\leq \theta \leq$ 3 mm, performed at U_∞ = 40 ms^{-1}. The result clearly shows that θ = 2 mm produced the greatest reduction in comparison to the other hole sizes for the three different configuration, with up to 3.5 dB for the x' = 4.4 mm and λ = 3

mm. In contrast, the smaller hole diameter θ = 0.7 mm produced only 1 dB noise reduction, furthermore, at larger $x' \geq$ 8.6 mm and $\lambda \geq$ 9 mm offered no phase cancellation with little to no noise increase or reduction. The largest porous hole diameter, θ = 3 mm, produced similar levels of noise reduction and slight increase in noise compared to the *theta* = 2 mm at x' = 8.6 mm and λ = 9 mm. However, at x' = 17 mm and λ = 15 mm produce significant noise increase up to 2.5 dB and little to no reduction. This suggests that the hole diameter influence the effectiveness of the eddies scattering into pressure waves and thus the level of phase cancellation between the single row of holes and the trailing edge.

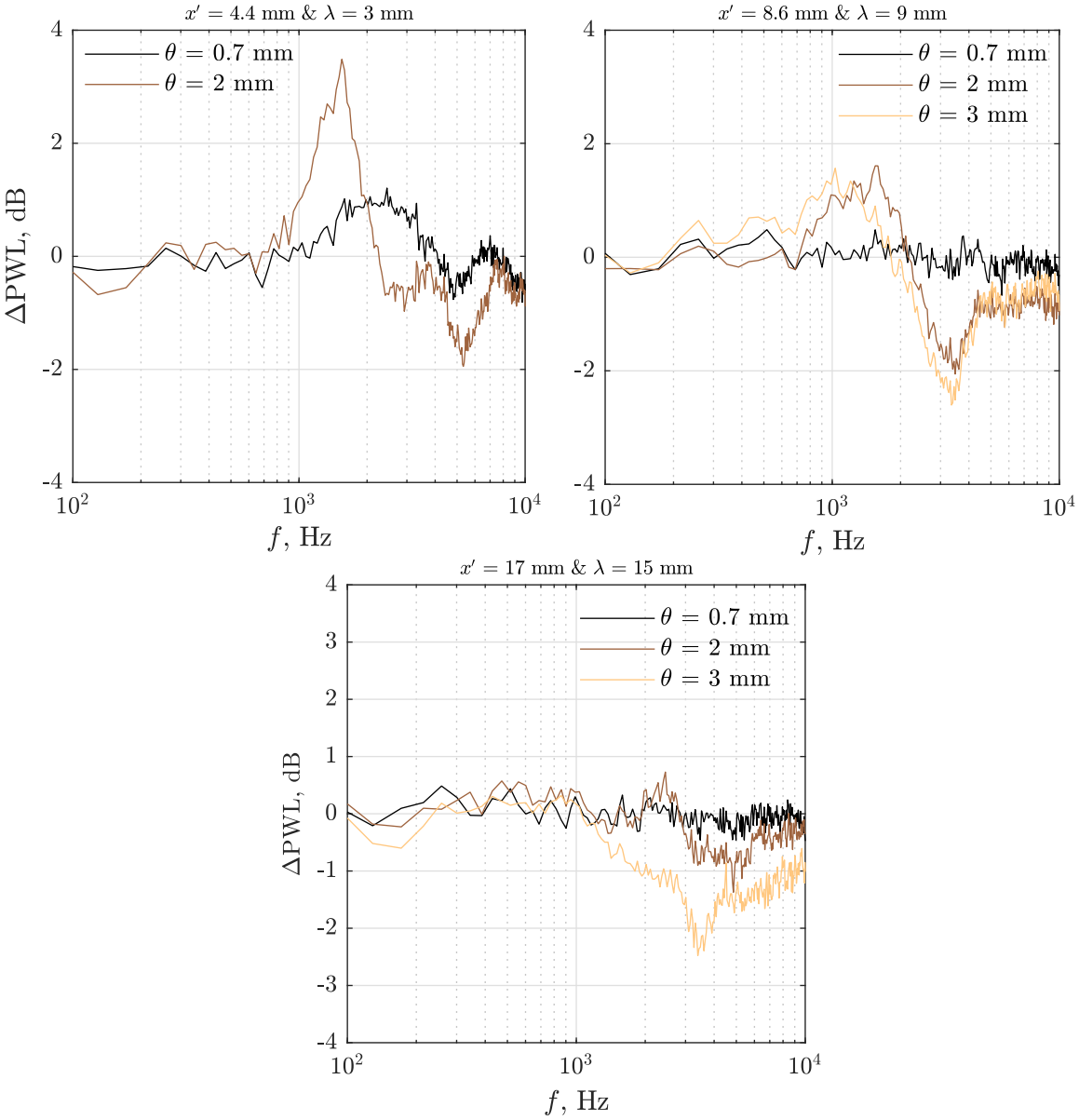

Fig. 9 Comparison of the ΔPWL, dB, between B and SINPLE trailing edge at θ = 0.7 mm, 2 mm and 3 mm for different x' and λ at U_∞ = 40 ms^{-1}.

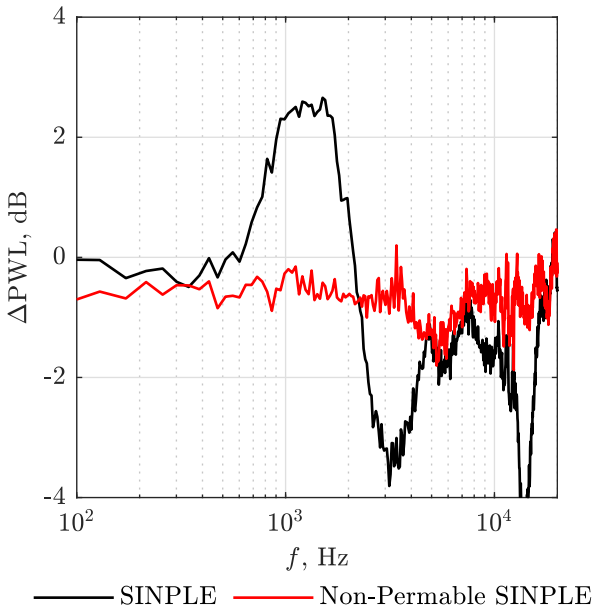

Fig. 10 Comparison of the permeable and non-permeable SINPLE trailing edge at x' = 8.6 mm, θ = 2 mm and λ = 3 mm at U_∞ = 40 ms^{-1}, where (a) ΔPWL, dB,

D. Derivative of the SINPLE trailing edge

1. Flow communication

Figure 10 showcase the effect of noise characteristics on permeable and non-permeable SINPLE trailing edge at 40 ms^{-1}. For the non-permeable case the pressure sided was taped. The results, as shown in Figure 10, demonstrated that non-permeable offered no noise reduction or acoustic interference between the two scattering sources. As explained in previous studies [7–9] that flow commutation between either side of the aerofoil is a necessary requirement for noise reduction. In terms of acoustic interference, the flow commutation is a necessary requirement to facilitate as a scattering location.

Figure 10b presents the non-dimensional velocity of the permeable, non-permeable and baseline trailing edge at U_∞ = 40 ms^{-1}. The result clearly showed a difference in the flow characteristics between the permeable and non-permeable trailing edge with permeable have a thinning within the viscous layer compare to the non-permeable. In comparison to the baseline, the non-permeable trailing edge results showed little-to-no change in the velocity.

2. Variation in the SINPLE Hole Angle

Figure 11 showcases the difference in sound power level, ΔPWL, against frequency for porous hole inclination. The inclination is based on the positions from the longitudinal displacement for the upper and lower surface, illustrated in Figure 11, where x'_U is kept at 8.6 mm. Firstly, it can be clearly seen that no inclination led to the largest noise reduction, up to 3.8 dB, amongst the other inclination cases. Secondly, the inclination angle greatly reduced the effects of phase cancellation with lowest reduction, up to 1 dB, achieved by the x'_U = 8.6 - x'_L = 14.2 mm. This suggest that the strength of the phase cancellation is reduced with hole inclination in both direction with similar effects. Furthermore, the frequency at which phase cancellation no longer collapse at St = 0.5, 1, 1.5, ... for either the x'_U or x'_L, however, instead collapse at longitudinal based on the average of the upper and lower hole locations: $\frac{x'_U + x'_L}{2}$. At the mid-to-high frequencies, the increased inclination angle of the porous holes resulted in increased noise level in comparison to the non-inclined cases with the exception for x'_U = 8.6 - x'_L = 3 mm case.

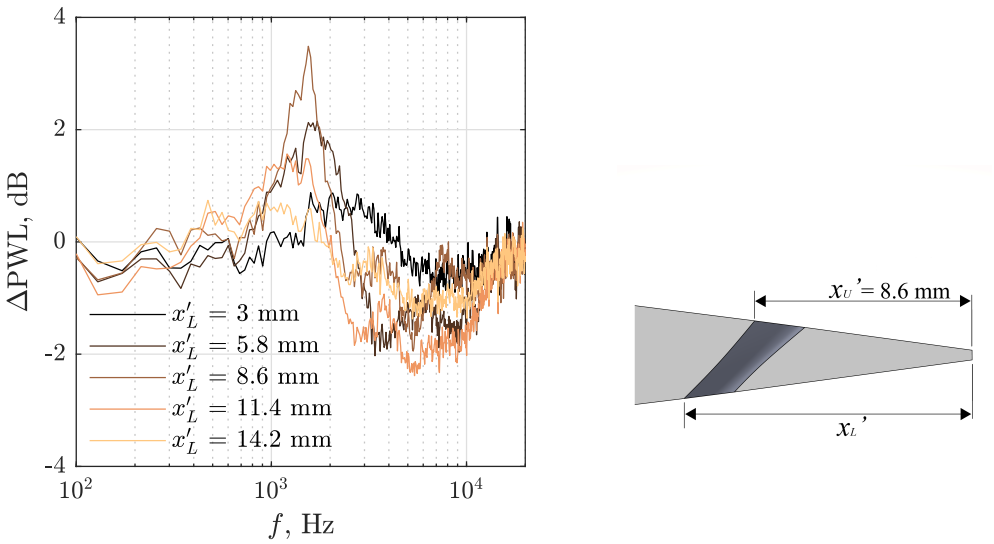

Fig. 11 Comparison of the ΔPWL, dB, between B and SINPLE trailing edge at θ = 0.7 mm, 2 mm and 3 mm for different x' and λ at U_∞ = 40 ms^{-1}.

3. Additional SINPLE

V. Summary

This paper investigates the effect of single row porous-arrangement at the trailing edge and their effects on the self-noise reduction of an aerofoil. The core technique employs in this paper is phase-cancellation between two sources that are physically displaced in a longitudinal direction. The mechanism employed known as destructive interference occurs between two sources that are 180° out-of-phase resulting in a cancellation. The far-field and near-field measurements of a NACA-0012 were conduction at the Brunel aero-acoustic facility, where two trailing edge configurations were investigated: Baseline (B) and Simple-Porous-Line (SINPLE). The SINPLE trailing eges were manufactured to cover a range of geometric parameters: longitudinal displacement, wavelength, hole diameter, and hole inclination. The experimental result successfully demonstrated co-existence of destructive and constructive interference at all freestream velocities and longitudinal displacements for the SINPLE trailing edge.

A noise prediction model successfully predicted the trends as well as

Furthermore, for all freestream cases, the highest noise reduction was consistently observed at the small longitudinal displacement, as well as the highest noise increase, where the largest reduction observed at x' = 4.4 mm up to 4 dB at U_∞ = 60 ms^{-1}.

Furthermore, the far-field noise measurements demonstrated that flow communication between either side trailing edge is necessary to facilitate acoustic interference. Finally, a analytical model

Acknowledgments

This work is supported by the UK Engineering and Phyiscal Sciences Research Council (EPSRC) research grant (EP/V006886/1) "Quiet Aerofoil with Adaptive Porous Surfaces (QUADPORS)". We also would like to express our appreciation to the PhD studentship funded by the EPSRC Doctoral Training Partnership (DTP) to the second author.

References

[1] Graham, R. R., "The Silent Flight of Owls," *The Journal of the Royal Aeronautical Society*, Vol. 38, No. 286, 1934, p. 837–843. https://doi.org/10.1017/S0368393100109915.

[2] Geyer, T., Sarradj, E., and Fritzsche, C., "Porous Airfoils: Noise Reduction and Boundary Layer Effects," *International Journal of Aeroacoustics*, Vol. 9, No. 6, 2010, pp. 787–820. https://doi.org/10.1260/1475-472X.9.6.787, URL https://doi.org/10.1260/1475-472X.9.6.787.

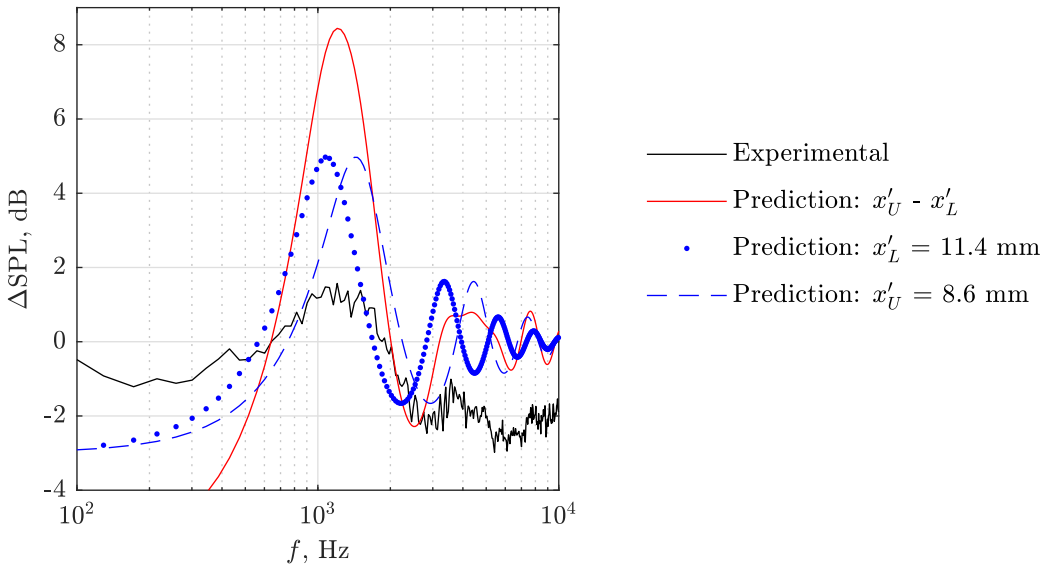

Fig. 12 Comparison of the ΔSPL, dB, between experimental and prediction of hole inclination with x'_L = 11.4 mm and x'_H = 5.7 mm, θ = 2 mm and λ = 3 mm at U_∞ = 40 ms^{-1}.

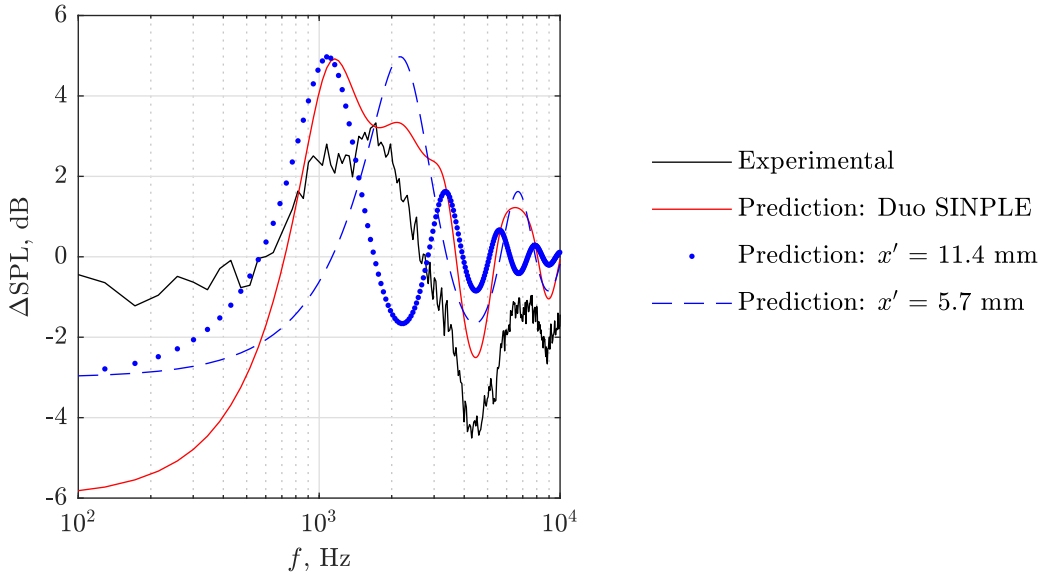

Fig. 13 Comparison of the ΔSPL, dB, between experimental and predicted duo SIPLE trailing edge with x' = 11.4 mm & 5.7 mm, θ = 2 mm and λ = 3 mm at U_∞ = 40 ms^{-1}.

[3] Sarradj, E., and Geyer, T., "Noise Generation by Porous Airfoils," *13th AIAA/CEAS Aeroacoustics Conference (28th AIAA Aeroacoustics Conference)*, 2007, pp. 1–13. https://doi.org/10.2514/6.2007-3719, URL https://arc.aiaa.org/doi/abs/10.2514/6.2007-3719.

[4] Geyer, T. F., and Sarradj, E., "Trailing Edge Noise of Partially Porous Airfoils," *20th AIAA/CEAS Aeroacoustics Conference*, 2017, pp. 1–18. https://doi.org/10.2514/6.2014-3039, URL https://arc.aiaa.org/doi/abs/10.2514/6.2014-3039.

[5] Rubio Carpio, A., Merino Martínez, R., Avallone, F., Ragni, D., Snellen, M., and van der Zwaag, S., "Experimental characterization of the turbulent boundary layer over a porous trailing edge for noise abatement," *Journal of Sound and Vibration*, Vol. 443, 2019, pp. 537–558. https://doi.org/https://doi.org/10.1016/j.jsv.2018.12.010, URL https://www.sciencedirect.com/science/article/pii/S0022460X18308277.

[6] Zhang, M., and Chong, T. P., "Experimental investigation of the impact of porous parameters on trailing-edge noise," *Journal of Sound and Vibration*, Vol. 489, 2020, p. 115694. https://doi.org/https://doi.org/10.1016/j.jsv.2020.115694, URL https://www.sciencedirect.com/science/article/pii/S0022460X20305241.

[7] Herr, M., Rossignol, K.-S., Delfs, J., Lippitz, N., and Mößner, M., "Specification of Porous Materials for Low-Noise Trailing-Edge Applications," *20th AIAA/CEAS Aeroacoustics Conference*, 2014, pp. 1–19. https://doi.org/10.2514/6.2014-3041, URL https://arc.aiaa.org/doi/abs/10.2514/6.2014-3041.

[8] Delfs, J., Faßmann, B., Lippitz, N., Lummer, M., Mößner, M., Müller, L., Rurkowska, K., and Uphoff, S., "SFB 880: aeroacoustic research for low noise take-off and landing," *CEAS Aeronautical Journal*, Vol. 5, 2014, pp. 403–417. https://doi.org/10.1007/s13272-014-0115-2.

[9] Rubio Carpio, A., Avallone, F., Ragni, D., Snellen, M., and van der Zwaag, S., "Mechanisms of broadband noise generation on metal foam edges," *Physics of Fluids*, Vol. 31, No. 10, 2019, p. 105110. https://doi.org/10.1063/1.5121248, URL https://doi.org/10.1063/1.5121248.

[10] Kim, J. W., Haeri, S., and Joseph, P. F., "On the reduction of aerofoil–turbulence interaction noise associated with wavy leading edges," *Journal of Fluid Mechanics*, Vol. 792, 2016, p. 526–552. https://doi.org/10.1017/jfm.2016.95.

[11] Chaitanya, P., and Joseph, P., "Slitted leading edge profiles for the reduction of turbulence-aerofoil interaction noise," *The Journal of the Acoustical Society of America*, Vol. 143, No. 6, 2018, pp. 3494–3504. https://doi.org/10.1121/1.5040972, URL https://doi.org/10.1121/1.5040972.

[12] van der Velden, W. C., Avallone, F., and Ragni, D., "Numerical analysis of noise reduction mechanisms of serrated trailing edges under zero lift condition," *23rd AIAA/CEAS Aeroacoustics Conference*, American Institute of Aeronautics and Astronautics, 2017. https://doi.org/10.2514/6.2017-4173.

[13] Woodhead, P. C., "Aerofoil self noise reduction by innovative trailing edge treatment," Phd thesis, Brunel University London, 2021. URL http://bura.brunel.ac.uk/handle/2438/23363.

[14] Woodhead, P. C., Chong, T. P., Joseph, P., and Wissink, J., "On the Double-Rooted Trailing Edge Serration," *25rd AIAA/CEAS Aeroacoustics Conference*, 2019, pp. 1–26. https://doi.org/10.2514/6.2019-2436, URL https://arc.aiaa.org/doi/abs/10.2514/6.2019-2436.

[15] Scholz, M. M., Chong, T. P., and Smith, E., "New strategy on porous trailing edge for self-noise reductions," *AIAA AVIATION 2021 FORUM*, 2017. https://doi.org/10.2514/6.2021-2109, URL https://arc.aiaa.org/doi/abs/10.2514/6.2021-2109.

[16] Amiet, R. K., "Noise due to turbulent flow past a trailing edge," *Journal of Sound and Vibration*, Vol. 47, No. 3, 1976, pp. 387 – 393. https://doi.org/10.1016/0022-460X(76)90948-2.

[17] Corcos, G. M., "Resolution of Pressure in Turbulence," *The Journal of the Acoustical Society of America*, Vol. 35, No. 2, 1963, pp. 192–199. https://doi.org/10.1121/1.1918431, URL https://doi.org/10.1121/1.1918431.

[18] Corcos, G., *Pressure fluctuations in shear flows*, No. 2 in 183, University of California, Institute of Engineering Research, 1962.

[19] Palumbo, D., "Determining correlation and coherence lengths in turbulent boundary layer flight data," *Journal of Sound and Vibration*, Vol. 331, No. 16, 2012, pp. 3721–3737. https://doi.org/10.1016/j.jsv.2012.03.015.

[20] Finnveden, S., Birgersson, F., Ross, U., and Kremer, T., "A model of wall pressure correlation for prediction of turbulence-induced vibration," *Journal of Fluids and Structures*, Vol. 20, No. 8, 2005, pp. 1127 – 1143. https://doi.org/https://doi.org/10.1016/j.jfluidstructs.2005.05.012, URL http://www.sciencedirect.com/science/article/pii/S0889974605000885.

[21] Meloni, S., Lawrence, J. L., Proença, A. R., Self, R. H., and Camussi, R., "Wall pressure fluctuations induced by a single stream jet over a semi-finite plate," *International Journal of Aeroacoustics*, 2020. https://doi.org/10.1177/1475472x20930650, URL https://doi.org/10.1177/1475472X20930650.